

Squeezing-enhanced resolution of radio-frequency signals

Wei Li (李卫)^{1,2}, Mingjian Ju (鞠明健)¹, Qinghui Li (李庆回)¹, Ruixin Li (李瑞鑫)¹, Wenxiu Yao (姚文秀)¹,
Yimiao Wu (武奕森)¹, Yajun Wang (王雅君)^{1,2}, Long Tian (田龙)^{1,2}, Shaoping Shi (史少平)^{1,2}, and
Yaohui Zheng (郑耀辉)^{1,2*}

¹State Key Laboratory of Quantum Optics and Quantum Optics Devices, Institute of Opto-Electronics, Shanxi University, Taiyuan 030006, China

²Collaborative Innovation Center of Extreme Optics, Shanxi University, Taiyuan 030006, China

*Corresponding author: yhzheng@sxu.edu.cn

Received December 8, 2023 | Accepted April 3, 2024 | Posted Online July 30, 2024

We demonstrate a resolution enhancement scheme of radio-frequency signals by tailoring a phase-squeezed state. The echo radio-frequency signals collected by photonic radar give rise to displacements in the phase quadrature of a probe laser and are estimated by the balanced homodyne detector. In contrast to the conventional coherent state, the noise variances for radio-frequency estimation with a squeezed state are reduced by approximately 6.9 dB. According to the Rayleigh criterion that defines the resolution limit, the minimum resolvable displacement Δa with a squeezed state is reduced to 45% compared to that with a coherent state, demonstrating the quantum advantage. The squeezing-enhanced technique has extensive applications for multitarget recognition and tracking in contemporary photonic radar systems.

Keywords: phase-squeezed state; radio-frequency signal; resolution.

DOI: [10.3788/COL202422.072701](https://doi.org/10.3788/COL202422.072701)

1. Introduction

Squeezing-enhanced technique (SET), which is a momentous branch of quantum metrology^[1–3], enables measurement sensitivity beyond the standard quantum limit (SQL)^[4–7]. Since proposed, massive efforts have been made to enhance the sensitivity of physical quantities including optical phase^[8,9], displacement^[10], rotation angle^[11], magnetic field^[12], and so on. Berni *et al.* demonstrated a quantum-enhanced optical phase estimation using squeezed vacuum states and real-time feedback control^[13]. Yonezawa *et al.* achieved the unprecedented precision for optical-phase tracking using a phase-squeezed state^[14]. Treps *et al.* and Sun *et al.* showcased subquantum noise level (sub-QNL) sensitivity in displacement measurements^[15,16]. Liu *et al.* realized rotating-angle measurement beyond the quantum limit^[17]. Li *et al.* obtained a 20% sensitivity improvement in an optomechanical magnetometer utilizing phase-squeezed light^[18]. Yap *et al.* reduced the quantum backaction noise by 1.2 dB with the injection of amplitude-squeezed light^[19]. Casacio *et al.* demonstrated a signal-to-noise ratio beyond the photodamage limit of conventional microscopy using bright quantum correlated illumination^[20]. Xia *et al.* demonstrated the entanglement-enhanced radio-frequency (RF) photonic sensing with a squeezing source and variable beam splitters^[21]. Recently, squeezed vacuum states have been tailored for advanced LIGO^[22] and advanced Virgo detectors^[23], enabling a 3 dB sensitivity enhancement.

Precise spatial resolution is of paramount significance to multitarget recognition, positioning, and tracking for military or civil radars^[24,25]. In order to achieve high spatial resolution, multiple radar systems have been proposed: for instance, the phased array antenna^[26], synthetic aperture radar^[27], microwave photonic radar^[28], millimeter-wave radar^[29], and so on. However, the existing photonic radars are not accurate enough to identify closely spaced targets. Therefore, it is always beneficial to improve the spatial resolution of photonic radar.

In this paper, we propose an innovative squeezing-enhanced photonic radar system, where the echo signals from closely spaced targets are simulated by RF signals, and the spatial resolution is enhanced by utilization of squeezed light. According to the Rayleigh criterion^[30–32], it offers a 55% resolution enhancement in contrast to that with coherent light.

2. Theoretical Analysis and Experimental Setup

Figure 1(a) illustrates the principle of squeezing-enhanced photonic radar. It commences with the introduction of a squeezed operator $\hat{S}(r, \theta)$, which generates a squeezed vacuum state by acting upon the vacuum state $|0\rangle$. Notably, the squeezed vacuum state has no coherent amplitude, and its noise fluctuation in phase quadrature is lower than the quantum noise limit (QNL)^[33–35]. At the signal acquisition module, the echo RF signal from the target is expressed as $E = A \sin(\Omega t + \phi)$, where A ,

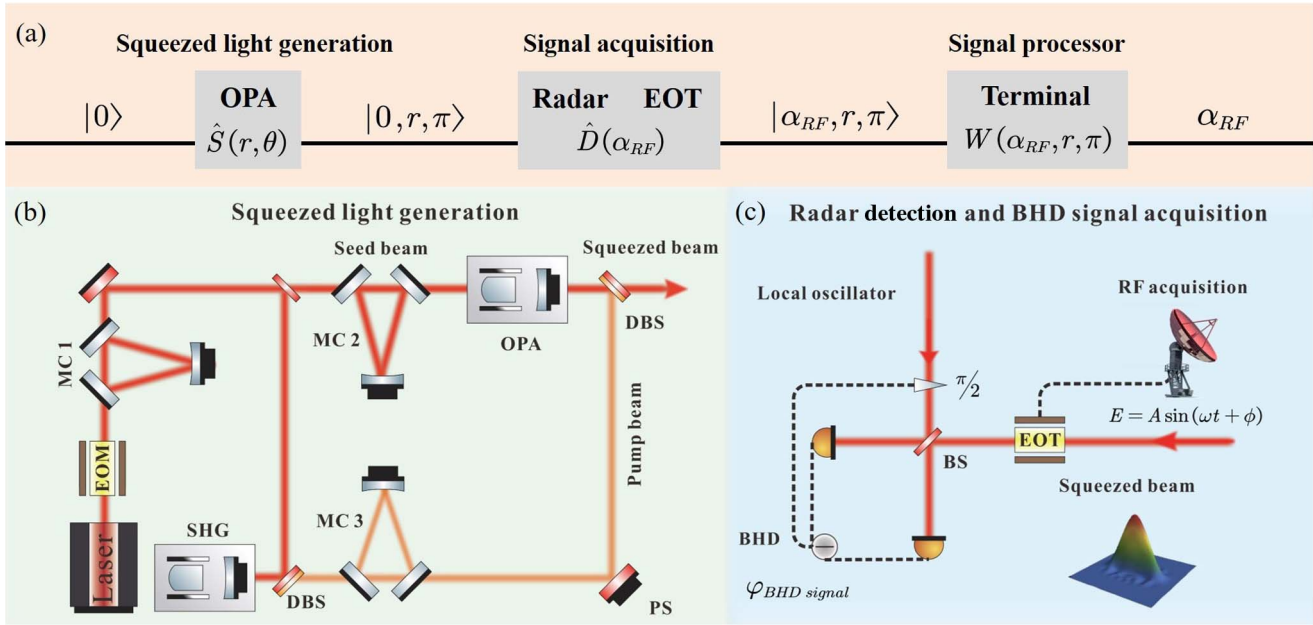


Fig. 1. (a) Represents the principle of the quantum-enhanced photonic radar system, comprising three main modules: squeezed light generation, signal acquisition, and signal processors. (b) depicts a module for squeezed light generation, while (c) illustrates the photonic radar RF acquisition and balanced homodyne detection. EOM, electro-optic modulator; MC, mode cleaner; OPA, optical parametric amplification; SHG, second-harmonic generation; PS, phase shifter; BS, beam splitter; DBS, dichroic beam splitter; BHD, balanced homodyne detector; EOT, electro-optic transducer; RF, radio-frequency.

Ω , and ϕ are the amplitude, frequency, and phase, respectively. The squeezing vacuum state is modulated by an electro-optical transducer (EOT) driven by the echo RF signal, introducing a displacement $\alpha_{RF} = A\kappa \sin(\phi)$ along the orthogonal phase axis in the phase space. Apparently, there is no displacement when the phase $\phi = 0$, while the maximum (minimum) displacement occurs at $\phi = \frac{\pi}{2}$ ($-\frac{\pi}{2}$). At the signal processing terminal, the displacement α_{RF} is measured by a balanced homodyne detector (BHD), from which we can acquire the amplitude and phase information of echo RF signals.

The experimental setup is depicted in Fig. 1(b). A continuous-wave single-frequency fiber laser at 1550 nm is injected into the mode cleaner1 (MC1), suppressing the intensity noise and phase noise for fundamental frequency while improving its beam quality. The output of MC1 is split into two beams, one of which traverses another mode cleaner2 (MC2), ulteriorly suppressing the noise. The other beam is subsequently resonant in the second-harmonic generation (SHG) resonator, where photons undergo parametric upconversion through the second-order nonlinear effect of the crystal, yielding a frequency-doubled light at 775 nm. For both 1550 and 775 nm, the front end of the crystal is highly reflective and the back end is antireflective. The output coupler is antireflective for 775 nm, while the transmissivity for 1550 nm is 12%. At the optimum phase-matching temperature, the maximum frequency doubling efficiency is 71%. A subset of the transmitted light of MC2 is designated as the seed beam for the optical parametric amplification (OPA) process, while the remainder serves as the local oscillator for the homodyne detection module. The seed beam and frequency-doubled laser are counterinjected into the OPA resonator, orchestrating the

parametric downconversion via a second-order nonlinear effect. The OPA is a half-monolithic resonator consisting of a concave mirror and a 10 mm periodically poled potassium titanyl phosphate (PPKTP) crystal. One end of the crystal is curved with a 12 mm radius and is highly reflective for both 1550 and 775 nm, while the opposite surface is antireflective for both wavelengths. The reflectivity of a concave mirror is 84.3% for 1550 nm and 97.8% for 775 nm, respectively. With a 21 mm air gap between the PPKTP crystal and the output mirror, the finesse of OPA is 35 for the 1550 nm and 200 for the 775 nm laser. In virtue of the doubly resonant characteristic of OPA, the cavity length is stabilized by frequency-doubled laser with meticulously designed proportional integral derivative (PID) feedback loop. The co-resonance condition for fundamental laser and frequency-doubled laser is satisfied by fine-tuning the temperature of the PPKTP crystal. By controlling the relative phase between seed beam and frequency-doubled laser to 0, a phase-squeezed light is generated with a maximum squeezing degree of $-7.1 \text{ dB} \pm 0.2 \text{ dB}$, while the antisqueezing degree is $10.0 \text{ dB} \pm 0.2 \text{ dB}$.

The RF signal acquired by photonic radar is transformed to a probe laser at the fundamental frequency by an EOT, introducing a displacement α_{RF} along the quadrature phase in phase space^[36,37]. In the experimental scenario, the unknown RF signal is simulated by a sinusoidal function whose frequency is 10 MHz. Subsequently, the probe laser is interfered with a strong local oscillator at a 50:50 beam splitter and injected towards the BHD. In order to access the displacement in phase quadrature, the relative phase between probe laser and local oscillator needs to be controlled at $\pi/2$. The desired information in the time domain is acquired by demodulating the AC output of BHD

with another sinusoidal function at 10 MHz and collected by a digital oscilloscope.

3. Experimental Results

Figure 2 contrasts the phase-squeezed state with the coherent state aiming at the estimation of RF phase. We initially estimated the RF phase utilizing the coherent state, which is generated by blocking the frequency-doubled laser for OPA. By automatically scanning the phase across 0 deg to 360 deg range with a step size of 10 deg, the averaged displacements are represented by the purple spheres, while the noise variances are displayed by the lavender shaded area. Subsequently, the phase-squeezed state is employed to estimate the RF phase. Sweeping the phase with the same parameters and collecting data automatically, the noise variances are illustrated by the dark purple shaded area. The black curve is a fitting for the experimental data, showing a sinusoidal pattern. Obviously, the noise variances for estimation of all RF phases are reduced by approximately 6.9 dB compared to that with the coherent state. Moreover, a gradient algorithm and a regional optimization algorithm are employed to locate the extremum of displacement measurements^[38]. As a result, the maximum and minimum displacements are represented by two red stars, corresponding to RF phases ϕ_1 and ϕ_2 , respectively.

Suppose two RF signals, $E_1 = A \sin(\Omega t + \phi_1)$ and $E_2 = A \sin(\Omega t + \phi_2)$, are echo signals from closely spaced targets, thus the distinguishability of E_1 and E_2 is of great significance for practical applications. It is worth mentioning that the ability to accurately resolve RF information hinges upon the noise variance of the displacement measurement. The higher noise variance will submerge the displacement signal and hinder accurate discernment. In order to achieve the minimum distinguishable RF signals, we decrease the RF amplitude until the noise

variances for two signals are interlacing. Moreover, when the phases of two RF signals are 0 or π , the first derivative of the sine function is the largest, corresponding to the point where phase estimation is most sensitive.

Figure 3(a) illustrates the estimated noise variances with the coherent state and corresponding Gaussian distribution curves. Figure 3(b) showcases the estimated noise variances with the squeezed state, and the corresponding probability distribution curves are also a Gaussian function. According to the Rayleigh criterion, which defines the resolution limit^[30–32], two RF signals are just resolvable when the central maximum of one Gaussian pattern is located at the minimum of the other. Therefore, the minimum resolvable displacement Δa with a coherent state can be normalized to unity, while the minimum resolvable displacement Δa with a squeezed state is reduced to 0.45. Figure 3(c) presents the relationship between resolvable displacement Δa and RF amplitude, making it possible to derive the RF amplitude from the displacement measurement. The red circles designate the experimental results for different RF amplitudes when the RF phases are fixed to ϕ_1 and ϕ_2 , whereas the dark purple line is fitting for experimental data. The light blue region showcases the RF amplitudes are distinguishable with the coherent state, while the dark blue region exhibits the distinguishable RF amplitude with the squeezed state. It is apparent that the distinguishable RF amplitude is diminished by harnessing the phase-squeezed state.

The resolution enhancement becomes notably evident upon reconstructing the Wigner function. To this end, the relative phase between the probe laser and local oscillator is scanned via a phase shifter. By setting the RF phases to ϕ_1 , 0, and ϕ_2 , respectively, the time-domain information for any quadrature is recorded by the oscilloscope. After extracting one complete cycle from the data, we derived the density matrix and Wigner function by employing the maximum likelihood (MaxLik) technique^[39]. Figure 4(a) showcases the reconstructed Wigner function and projection in phase space while employing the coherent state to estimate the RF signal. The red region represents the most densely concentrated area within the phase space. Apparently, three RF signals are superposing together and indistinguishable when the coherent state is acting as a probe.

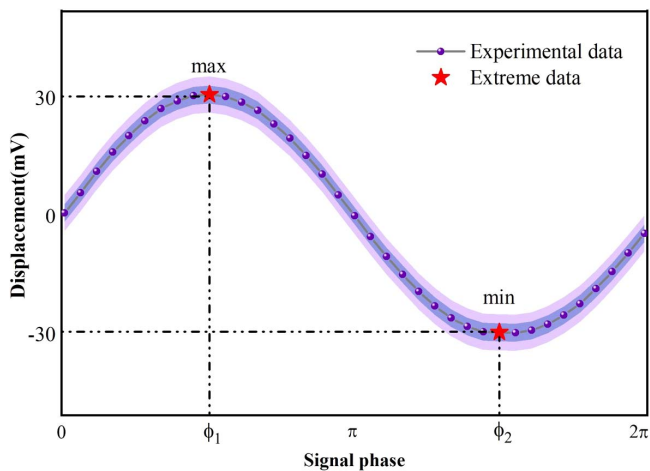


Fig. 2. The displacement measurement by fixing the RF amplitude and automatically scanning the RF phase. The purple spheres: the measured displacement for different RF phases; the black curve: a sinusoidal fitting for experimental data; the shaded area, the noise variances of the estimation results.

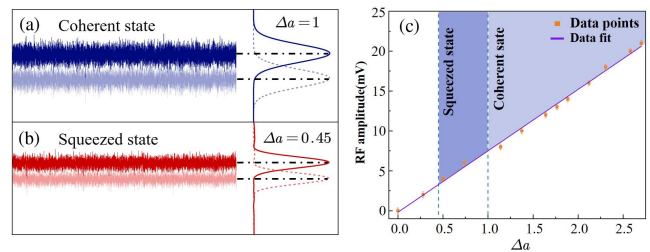


Fig. 3. (a) The estimated noise variances with the coherent state by fixing the RF phase to ϕ_1 (dark blue) and ϕ_2 (light blue). (b) The estimated noise variances for RF phases ϕ_1 (dark red) and ϕ_2 (light red) with the squeezed state. (c) The contrast of distinguishable RF amplitudes by utilizing the squeezed state and the coherent state.

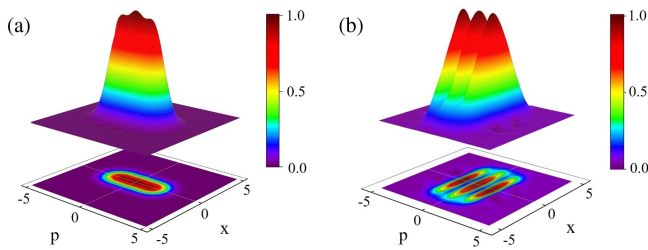


Fig. 4. The reconstructed Wigner function for RF signal estimation with the (a) coherent state and (b) phase-squeezed state.

Figure 4(b) displays the Wigner function and projection in phase space arising from the estimation results with the squeezed state. In contrast, three RF signals are discernible clearly by utilizing the phase-squeezed state, underscoring a 55% enhancement in spatial resolution compared to that with the coherent state.

4. Conclusion

We have demonstrated a 55% enhancement in the resolution of RF signals by tailoring a phase-squeezed state with a squeezing degree of -7.1 dB. The echo RF signals from the target lead to displacements in the phase quadrature of the probe laser and are estimated by a BHD. In contrast to traditional coherent light sources, the noise variances for RF estimation with the squeezed state are reduced by approximately 6.9 dB. According to the Rayleigh criterion, the minimum resolvable displacement Δa with the squeezed state is reduced to 0.45 when Δa with the coherent state is normalized to unity, demonstrating the quantum advantage. Automated scanning techniques accelerate the experimental process and improve the effectiveness of data acquisition. The proposed methodology holds significant promise for multitarget recognition and tracking in current photonic radar systems.

Acknowledgements

This work was supported by the National Natural Science Foundation of China (Nos. 62225504, 12274275, 62027821, U22A6003, 62035015, 62375162, 12304399, and 12174234), the Key R&D Program of Shanxi (No. 202302150101015), and the Fundamental Research Program of Shanxi Province (Nos. 202303021212003 and 202303021224006).

References

- V. Giovannetti, S. Lloyd, and L. Maccone, "Quantum metrology," *Phys. Rev. Lett.* **96**, 010401 (2006).
- V. Giovannetti, S. Lloyd, and L. Maccone, "Advances in quantum metrology," *Nat. Photonics* **5**, 222 (2011).
- L. J. Fiderer and D. Braun, "Quantum metrology with quantum-chaotic sensors," *Nat. Commun.* **9**, 1351 (2018).
- L. W. Wang and J. Shi, "Quantum fluctuation and interference effect in a single atom-cavity QED system driven by a broadband squeezed vacuum," *Chin. Opt. Lett.* **18**, 122701 (2020).
- W. H. Stefan and W. Jan, "Breaking the diffraction resolution limit by stimulated emission: stimulated-emission-depletion fluorescence microscopy," *Opt. Lett.* **19**, 780 (1994).
- Y. M. Wu, Q. W. Wang, L. Tian, *et al.*, "Multi-channel multiplexing quantum teleportation based on the entangled sideband modes," *Photonics Res.* **10**, 1909 (2022).
- Y. X. Chen, Q. Q. Zhu, X. T. Wang, *et al.*, "Deterministic all-optical quantum state sharing," *Adv. Photonics* **5**, 026006 (2023).
- T. A. Wheatley, D. W. Berry, H. Yonezawa, *et al.*, "Adaptive optical phase estimation using time-symmetric quantum smoothing," *Phys. Rev. Lett.* **104**, 093601 (2010).
- K. Zhang, S. S. Liu, Y. X. Chen, *et al.*, "Optical quantum states based on hot atomic ensembles and their applications," *Photonics Insights* **1**, R06 (2022).
- N. Treps, N. Grosse, W. P. Bowen, *et al.*, "A quantum laser pointer," *Science* **301**, 940 (2003).
- V. Delaubert, N. Treps, M. Lassen, *et al.*, "TEM10 homodyne detection as an optimal small-displacement and tilt-measurement scheme," *Phys. Rev. A* **74**, 053823 (2006).
- D. V. Kupriyanov and I. M. Sokolov, "Optical detection of magnetic-resonance by classical and squeezed light," *Quantum Opt.* **4**, 55 (1992).
- A. A. Berni, T. Gehring, B. M. Nielsen, *et al.*, "Ab initio quantum-enhanced optical phase estimation using real-time feedback control," *Nat. Photonics* **9**, 577 (2015).
- H. Yonezawa, D. Nakane, T. A. Wheatley, *et al.*, "Quantum-enhanced optical-phase tracking," *Science* **337**, 1514 (2012).
- N. Treps, U. Andersen, B. Buchler, *et al.*, "Surpassing the standard quantum limit for optical imaging using nonclassical multimode light," *Phys. Rev. Lett.* **88**, 203601 (2002).
- H. X. Sun, Z. L. Liu, K. Lui, *et al.*, "Experimental demonstration of a displacement measurement of an optical beam beyond the quantum noise limit," *Chin. Phys. Lett.* **31**, 084202 (2014).
- K. Liu, C. X. Cai, J. Li, *et al.*, "Squeezing-enhanced rotating-angle measurement beyond the quantum limit," *Appl. Phys. Lett.* **113**, 261103 (2018).
- B. B. Li, J. Bílek, U. B. Hoff, *et al.*, "Quantum enhanced optomechanical magnetometry," *Optica* **5**, 850 (2018).
- M. J. Yap, J. Cripe, G. L. Mansell, *et al.*, "Broadband reduction of quantum radiation pressure noise via squeezed light injection," *Nat. Photonics* **14**, 19 (2020).
- C. A. Casacio, L. S. Madsen, A. Terrasson, *et al.*, "Quantum-enhanced nonlinear microscopy," *Nature* **594**, 201 (2021).
- Y. Xia, W. Li, W. Clark, *et al.*, "Demonstration of a reconfigurable entangled radio-frequency photonic sensor network," *Phys. Rev. Lett.* **124**, 150502 (2022).
- M. Tse, H. C. Yu, N. Kijbunchoo, *et al.*, "Quantum-enhanced advanced LIGO detectors in the era of gravitational-wave astronomy," *Phys. Rev. Lett.* **123**, 231107 (2019).
- F. Acernese, M. Agathos, L. Aiello, *et al.*, "Increasing the astrophysical reach of the advanced Virgo detector via the application of squeezed vacuum states of light," *Phys. Rev. Lett.* **123**, 231108 (2019).
- A. Moccia and A. Renga, "Spatial resolution of bistatic synthetic aperture radar: impact of acquisition geometry on imaging performance," *IEEE Trans. Geosci. Remote* **49**, 3487 (2011).
- G. F. Zheng, F. Patolsky, Y. Cui, *et al.*, "Multiplexed electrical detection of cancer markers with nanowire sensor arrays," *Nat. Biotechnol.* **23**, 1294 (2005).
- R. J. Mailloux, "Phased array theory and technology," *Proc. IEEE* **70**, 246 (1982).
- N. A. Goodman and J. M. Stiles, "Resolution and, synthetic aperture characterization of sparse radar arrays," *IEEE Trans. Aerosp. Electron. Syst.* **39**, 921 (2003).
- S. L. Pan and Y. M. Zhang, "Microwave photonic radars," *J. Light. Technol.* **38**, 5450 (2020).
- J. Hasch, E. Topak, R. Schnabel, *et al.*, "Millimeter-wave technology for automotive radar sensors in the 77 GHz frequency band," *IEEE Trans. Microwave Theory Tech.* **60**, 845 (2012).
- M. Tsang, R. Nair, and X. M. Lu, "Quantum theory of superresolution for two incoherent optical point sources," *Phys. Rev. X* **6**, 031033 (2016).

31. F. Yang, A. Tashchilina, E. S. Moiseev, *et al.*, "Far-field linear optical super-resolution via heterodyne detection in a higher-order local oscillator mode," *Optica* **3**, 1148 (2016).
32. S. W. Hell and J. Wichmann, "Breaking the diffraction resolution limit by stimulated emission: stimulated-emission-depletion fluorescence microscopy," *Opt. Lett.* **19**, 780 (1994).
33. X. C. Sun, Y. J. Wang, L. Tian, *et al.*, "Detection of 13.8 dB squeezed vacuum states by optimizing the interference efficiency and gain of balanced homodyne detection," *Chin. Opt. Lett.* **17**, 072701 (2019).
34. V. Giovannetti, S. Lloyd, and L. Maccone, "Quantum-enhanced measurements: beating the standard quantum limit," *Science* **306**, 1330 (2004).
35. Y. J. Wang, Y. H. Tian, X. C. Sun, *et al.*, "Noise transfer of pump field noise with analysis frequency in a broadband parametric downconversion process," *Chin. Opt. Lett.* **19**, 052703 (2021).
36. X. C. Sun, W. Li, Y. H. Tian, *et al.*, "Quantum positioning and ranging via a distributed sensor network," *Photonics Res.* **10**, 2886 (2022).
37. W. Li, X. C. Sun, Y. H. Tian, *et al.*, "Quantum-enhanced angle-of-arrival pre-estimation of radio-frequency signals," *Opt. Laser Technol.* **166**, 109643 (2023).
38. P. Baldi, "Gradient descent learning algorithm overview: a general dynamical systems perspective," *IEEE Trans. Neural. Netw. Learn Syst.* **6**, 182 (1995).
39. A. I. Lvovsky and M. G. Raymer, "Continuous-variable optical quantum-state tomography," *Rev. Mod. Phys.* **81**, 299 (2009).